Journal of the Mechanical Behavior of Biomedical Materials 90 (2019) 30–39

Contents lists available at ScienceDirect

Journal of the Mechanical Behavior of Biomedical Materials

journal homepage: www.elsevier.com/locate/jmbbm

Effect of water concentration on the shock response of polyethylene glycol diacrylate (PEGDA) hydrogels: A molecular dynamics study

Ke Luo[a], Noah Yudewitz[b], Ghatu Subhash[b], Douglas E. Spearot[b,*]

[a] Department of Materials Science & Engineering, University of Florida, United States
[b] Department of Mechanical & Aerospace Engineering, University of Florida, United States

ARTICLE INFO

Keywords:
Shock
Hydrogels
Molecular dynamics
Water concentration
PEGDA

ABSTRACT

Shockwave propagation in polyethylene glycol diacrylate (PEGDA) hydrogels is simulated for the first time using nonequilibrium molecular dynamics simulations. PEGDA hydrogel models are built using the "perfect network" approach such that each crosslink junction is comprised of six chain connections. The influence of PEGDA concentration (20–70 wt%) on shock behavior is investigated for a range of particle velocities (200–1000 m/s). In agreement with reported experimental results in the literature on gels with similar densities, shock velocity and pressure in PEGDA hydrogels are found to increase with polymer concentration, within a range bounded by pure water and pure polymer behaviors. Nonlinear relationships are observed for shock pressure and shock front thickness as a function of concentration, and a logarithmic equation is proposed to describe this behavior. In addition, the relationship between pressure and shock front thickness is compared with hydrodynamic theory. Deviation from hydrodynamic predictions is observed at high particle velocities and this deviation is found to be related to viscosity changes. A power-law relationship between strain rate and pressure in PEGDA hydrogels is identified, similar to that of metals. However, a power-law exponent of 1.4 is computed for all gel concentrations, whereas an exponent of 4 is typically reported for metals.

1. Introduction

Hydrogels are composite materials that consist of cross-linked polymer networks swollen in water or biological fluids (Haraguchi, 2007). Their low stiffness and controllable permeability enable a wide range of applications in biomedical and pharmaceutical fields (Hoare and Kohane, 2008; Puoci and Curcio, 2013), such as in space filling scaffolds and bioactive molecule delivery systems. Because hydrogels can have similar viscoelastic behavior to human tissue, they may be used to simulate tissue injuries under various deformation modes (Elsherbiny and Yacoub, 2013; Drury and Mooney, 2003). While research has been conducted to study the mechanical properties of hydrogel simulants at quasi-static or low strain rate conditions (Kwon and Subhash, 2010; Richler and Rittel, 2014; Naarayan and Subhash, 2017; Subhash et al., 2011), those experimental results are not applicable to hydrogels under high strain rate impact characteristic of ballistic injuries, because the mechanical response of polymeric materials, including hydrogels, at high strain rate is significantly different than that at low strain rate (Doman et al., 2006; Cronin and Falzon, 2009; Forte et al., 2015; Vliet, 1995; Subhash et al., 2012).

Investigations into the dynamic response of hydrogels beyond 10^5 s^{-1} strain rate, where a shockwave occurs, are limited (Patel et al., 1992; Demirci and Khademhosseini, 2016; Muniz and Geuskens, 2001; Shepherd et al., 2009; Appleby-Thomas et al., 2014; Toyoda and Gupta, 2014). The primary focus of prior work was on the shock Hugoniot relationship of hydrogels where experimental results are compared with predictions made via the conservation laws associated with the hydrodynamic approximation (Grady, 2017). For example, Anderson et al. (2017) found that the Tait equation of state can accurately predict shock pressure of 5 wt% Gellan gum hydrogel within 2% error. Appleby-Thomas et al. (2014) obtained the pressure versus density Hugoniot of several tissue simulants and found that 25 wt% gelatin made of porcine skin powder abides by the hydrodynamic prediction. This observation was further extended to ballistic gels with different gelatin concentrations by Toyoda and Gupta (2014). They compared the shock responses of 10 and 20 wt% ballistic gels subjected to particle velocities up to 400 m/s and noted that both shock velocity and pressure increased with gelatin concentration. It was postulated that the increase in bulk sound velocity and density at higher gelatin concentrations accounted for the differences in shock responses. However, only two concentrations were investigated; thus, the detailed relationship between shock response and concentration is still unknown.

* Corresponding author.
E-mail address: dspearot@ufl.edu (D.E. Spearot).

https://doi.org/10.1016/j.jmbbm.2018.09.017
Received 13 July 2018; Received in revised form 12 September 2018; Accepted 14 September 2018
Available online 15 September 2018

The hydrodynamic approximation assumes that the shock front is a discontinuity (Landau and Lifshitz, 1987), but previous studies of shockwave propagation in a range of materials (Holian, 1998; Holian et al., 1980; Hoover, 1979; Brown et al., 2007; Hess, 1997) indicated that a smooth transition region is observed at the shock front, defined as the shock front thickness. An extended hydrodynamic function was proposed (Hess, 1997) that includes the effects of dissipation mechanisms, such as viscosity and thermal conductivity, to provide an approach to characterize the shock front thickness as a function of shock pressure. However, shock front thickness and potential deviations from hydrodynamic theory have not been addressed in hydrogels. Furthermore, a power-law relationship between strain rate and stress with an exponent of 4 is observed in experiments on many solid materials, typically metals. This is commonly known as the "fourth power-law" (Grady, 2010). Deviations from this relationship are reported in composite materials, and as hydrogels are a type of composite material, it is necessary to explore the applicability of power-law relationships between strain rate and stress in hydrogels. Therefore, the objective of this research is to investigate the influence of concentration on the dynamic behavior of hydrogels, including the shock Hugoniot and shock front thickness during shockwave propagation, with a special focus on the applicability of hydrodynamic theory and power-law relationships to hydrogels.

Experimental investigations into the shock response of hydrogels are expensive and limited by the resolution of the equipment. The molecular dynamics (MD) simulation method, which provides atomic scale details of the interaction and motion of atoms, is commonly used as a tool to explore beyond experimental capabilities. To date, MD simulations have not been used to study shockwave propagation in hydrogels. However, this method has been used to extract shock relationships in many other material systems. For example, early nonequilibrium MD simulations of strong shockwaves in Lennard-Jones liquids found that simulation results of density, temperature and pressure agree with predictions based on a Navier-Stokes model (Holian et al., 1980). The structure of polyvinylchloride (PVC) polymer under shock loading was investigated by Neogi and Mitra (2016) They found a bond dissociation mechanism that decreases the slope of the temperature versus mean stress Hugoniot after PVC reaches the glass transition temperature. Investigations of this type provide a foundation to apply MD simulations to study shock in hydrogels. Thus, this research uses nonequilibrium MD simulations to simulate the shock responses of hydrogels with various concentrations. All simulations are performed using the LAMMPS code.

This paper is organized into four sections. Section 2 describes the selection of hydrogel material and force fields, construction of hydrogel models and methods for conducting shock simulations. Section 3 provides Hugoniot relationships for shock velocity, pressure and their comparisons with experiments. The relationship between shock front thickness, pressure and viscosity are explored. The influence of hydrogel concentration is investigated in each relationship. Section 4 summaries the work and provides conclusions.

2. Simulation setup

2.1. Hydrogel chemistry

A major challenge to model hydrogels is the complexity of most hydrogel networks. The polyethylene glycol diacrylate (PEGDA) hydrogel is used in this research because it has representative features, such as a simple covalently bonded crosslinked network, and sufficient experimental data is available to validate the models. PEGDA is a synthetic polymer that can be crosslinked by photochemical or redox initiated free radical polymerization, where the diacrylate group serves as the crosslinking agent. Previous experiments and simulations have provided data of mesh size (Ju et al., 2009), equilibrium density (Witte et al., 2004), water concentration and elastic modulus (Jang and Goddard, 2007) for PEGDA hydrogels. Those data are useful in this research to validate model construction and equilibration results. Note, hydrogels commonly studied in ballistics/shock experiments have a more complex structure; for example, collagen as the main component of ballistic gelatin has a triple helix structure (Sperling, 2006) that has not been successfully modeled yet in MD simulations.

2.2. Force fields

Since PEGDA hydrogels contain significant amounts of water (Okay, 2009), the accuracy of the interatomic potential for water molecules is critical for the hydrogel simulation. Water force fields such as SPC/E (Berendsen et al., 1987), TIP3P (Fischer and Karplus, 1996; Jorgensen et al., 1983) and TIP4P (Abascal and Vega, 2005; González and Abascal, 2011) with rigid and flexible styles are compared via hydrostatic compression tests in a cubic simulation cell with 42,700 water molecules. Both TIP4P flexible and TIP3P flexible potentials predict less than 2% error in equilibrium density (0.996 g/cm^3) and less than 3% error in bulk modulus (2.538 GPa) as compared with IAPWS-95 standards. The TIP3P flexible potential is more computationally efficient because no additional charge center is required. Thus, this study utilizes the flexible TIP3P (Liew et al., 1998) potential to model oxygen and hydrogen atoms explicitly in water within the hydrogel.

Interatomic potentials for polymers are generally divided into reactive force fields, such as ReaxFF (Van Duin et al., 2001), and nonreactive force fields, such as OPLS (Rizzo and Jorgensen, 1999; Jorgensen et al., 1984). Prior research has indicated that, although reactive force fields allow for bond-breaking and other reactive actions, their computational cost can be 30 times more than the nonreactive OPLS force field (Mattsson et al., 2010). Considering that the models used for shock simulations in this work are on the order of millions of atoms, the PEGDA polymer chains in this study are modeled using the OPLS united-atom force field to reduce computational cost. In the OPLS united-atom force field, the methyl groups are combined into a united atom. The total potential energy has the following form,

$$U_{total} = U_{nonbond} + U_{bond} + U_{angle} + U_{dihedral} + U_{improper} \quad (1)$$

where the subscripts *bond*, *angle*, *dihedral* and *improper* interactions are modeled by harmonic styles (Rizzo and Jorgensen, 1999). The nonbonded energy is calculated by the function,

$$U_{nonbond} = 4\epsilon\left[\left(\frac{r_e}{r}\right)^{12} - \left(\frac{r_e}{r}\right)^{6}\right] + k_{coul}\frac{q_i q_j}{r} \quad (2)$$

where r is the distance between atoms i and j, r_e is the equilibrium distance, ϵ and k_{coul} are the energy coefficients and q is the partial charge. A cut-off distance of 10 Å is applied in equilibration and shockwave simulations for the Lennard-Jones contribution. The particle-particle particle-mesh (PPPM) method is used as the long-term Coulomb corrections.

2.3. Construction of a perfect network hydrogel model

The "perfect network" model (Sun and Zhou, 2012; Lee et al., 2009; Wu et al., 2009) refers to a hydrogel structure in which all chain ends are connected to a unique node, and all nodes have exactly six chain connections. Although this model ignores the distribution of crosslinks and defects in hydrogels, preliminary studies have suggested that results using this model concur with experimental data regarding elastic modulus (Lee et al., 2009) and density (Jang and Goddard, 2007). As this is the initial study of its kind, this work uses the perfect network to model the shock response of PEGDA hydrogels. PEGDA with degree of polymerization (DP) of 13 and 23, denoted as PEGDA13 and PEGDA23, are created using Moltemplate. A crosslinked junction with six PEGDA chains is placed at the center of a simulation cell. Each PEGDA chain breaks the double bond of the inner-side acrylate group and connects

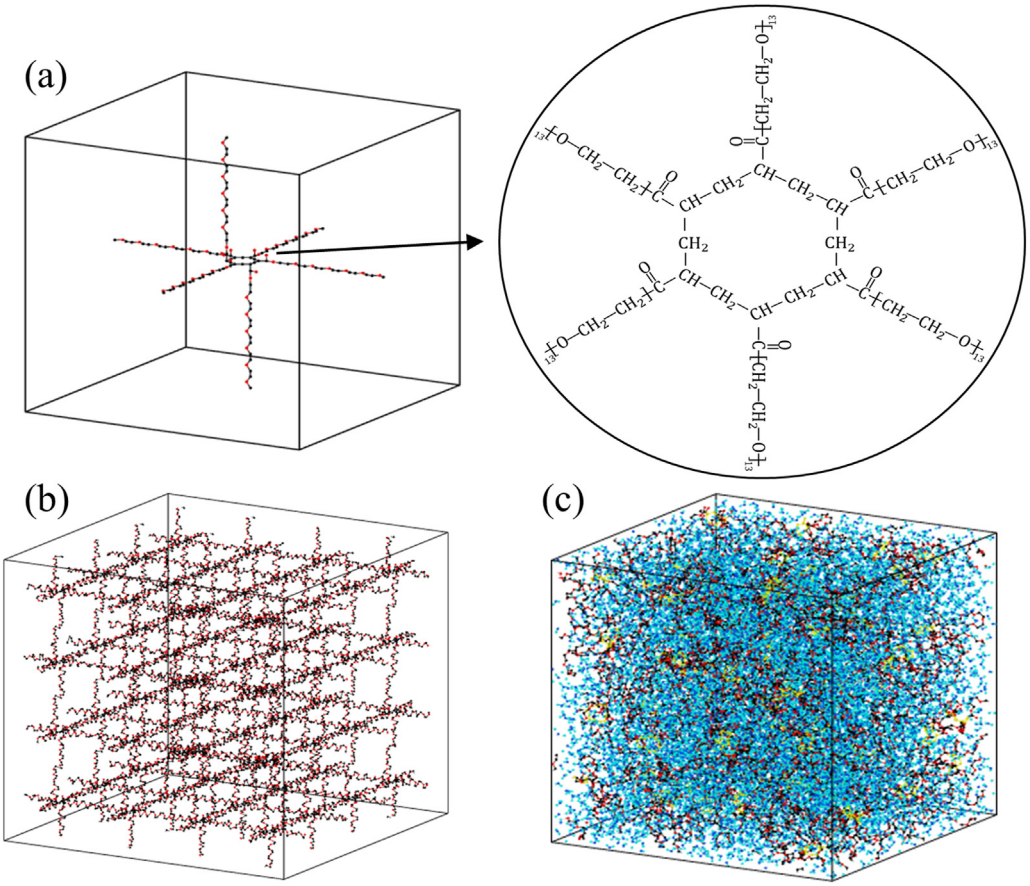

Fig. 1. Schematic representation of the perfect network model (a) before replication showing the ideal structure for the junction, (b) after replication in three dimensions, and (c) after equilibration with water molecules.

with the neighbor PEGDA chain in the junction as a closed ring structure. This structure as a crosslinked junction is fully extended in six directions. To make the model statistically representative, the crosslinked junction is replicated 5 times in x and y directions, and 75 times in the z direction (shock direction) with periodic boundary conditions in all directions. Water molecules are inserted into the simulation box after replication to create hydrogel models with 20–70 wt% PEGDA. All results are presented in terms of PEGDA concentration unless otherwise noted. Fig. 1 shows schematic representations of the junction replication and water insertion procedures in a cubic box. Three statistically different hydrogel models are created at each water concentration, using different random seed numbers for water molecule insertion and temperature initialization. Model equilibration is performed in the isothermal-isobaric (NPT) ensemble at 298 K and 1 atm for 300 ps, where thermodynamic properties such as temperature, pressure and density are used to decide whether the equilibrium state is reached. The equilibrium sizes of PEGDA13 models range from 1050 Å to 2025 Å in z direction, and 70 Å to 130 Å in lateral directions depending on water concentrations. The average mesh size of the hydrogel is calculated as the length of the equilibrated model divided by the repeating units in that direction, then averaged in three directions.

The average density and mesh size of perfect network models in equilibrium along with experimental data for PEGDA13 hydrogels (Ju et al., 2009; Witte et al., 2004) are shown in Table 1. Models with only water and only PEGDA polymer are also built as reference points. The error is computed as the maximum difference from the average value of three statistically different models. The equilibration procedures using the TIP3P and OPLS force fields capture the same trend as in experiments (Ju et al., 2009). Specifically, equilibrium density increases and mesh size decreases in hydrogels with higher polymer concentrations.

Table 1
Equilibrium mesh sizes and densities of PEGDA13. Note that hydrogel concentrations are presented in terms of water content to be consistent with experiments.

Water content (wt%)	Mesh size (Å)		Density (g/cm^3)	
	Simulation	Experiment (Ju et al., 2009)	Simulation	Experiment (Witte et al., 2004)
100	N/A	N/A	0.992 ± 0.001	0.996
80	26.3 ± 0.2	N/A	1.007 ± 0.001	1.021
70	21.8 ± 0.1	23	1.019 ± 0.002	1.043
60	19.9 ± 0.1	17	1.043 ± 0.002	1.067
50	18.7 ± 0.1	15	1.063 ± 0.001	1.083
40	17.3 ± 0.1	13	1.096 ± 0.002	1.103
30	15.9 ± 0.1	N/A	1.133 ± 0.001	1.123
0	14.1 ± 0.1	N/A	1.184 ± 0.001	1.183

The equilibrium densities from MD simulations concur with experiments (Witte et al., 2004), where the maximum percentage error is 2% in the hydrogel model with 70 wt% water. The MD simulation mesh sizes have better agreement with experiments at higher water concentrations. But, at lower water concentrations, average mesh sizes from experiment decrease faster than that in simulations. Experimental samples with higher PEGDA concentrations likely contain a higher density of network defects and those defects promote lower average mesh sizes, while the perfect model used here does not have defects.

Table 2 shows the comparison between density and mesh size for PEGDA13 and PEGDA23 hydrogels at equilibrium. Minimal differences are computed for density, where the maximum difference is 1.5% in hydrogels with 60 wt% water. All PEGDA23 hydrogels have a higher

Table 2
Equilibrium mesh sizes and densities of PEGDA13 and 23 hydrogels. Note that hydrogel concentrations are presented in terms of water content.

Water content (wt %)	Mesh size (Å)		Density (g/cm^3)	
	PEGDA13	PEGDA23	PEGDA13	PEGDA23
70	21.8 ± 0.1	27.1 ± 0.1	1.019 ± 0.002	1.021 ± 0.001
60	19.9 ± 0.1	24.5 ± 0.1	1.043 ± 0.002	1.028 ± 0.002
50	18.7 ± 0.1	22.8 ± 0.1	1.063 ± 0.001	1.054 ± 0.003
40	17.3 ± 0.1	21.0 ± 0.1	1.096 ± 0.002	1.085 ± 0.001
30	15.9 ± 0.1	19.7 ± 0.1	1.133 ± 0.001	1.125 ± 0.001

mesh size than PEGDA13 hydrogels, with an average difference of 4.5 Å. This is expected, as the higher degree of polymerization in PEGDA23 hydrogels naturally leads to an increase in mesh size with concurrent reduction in density at higher polymer concentrations.

2.4. Shockwave propagation

There are two common methods to conduct shock studies using MD (Holian, 1998). The multiscale shock technique (MSST) controls the volume and temperature of the simulation cell to restrain the system to the Hugoniot energy condition and Rayleigh line. This method is computationally efficient because it does not require a large model; however, this method does not allow for an analysis of key shockwave details, such as the shock front thickness and strain rate, which are both important aspects for this study. Thus, this study uses the non-equilibrium momentum mirror method to generate a shockwave propagating through a large simulation cell, as shown in Fig. 2. The periodic boundary is removed in the z direction, a particle velocity $-U_p$ from 200 m/s to 1000 m/s is added to the current velocity of each atom in the equilibrated hydrogel model, and the momentum mirror is placed at the $z = 0$ plane. Atoms impacting the momentum mirror are perfectly reflected back into the simulation cell with an opposite velocity generating a shockwave at the $z = 0$ plane propagating in the positive z direction. MD simulations of shock are conducted in the microcanonical (NVE) ensemble.

The hydrogel model is divided into 3000 thin bins along the z direction. This bin resolution is determined via preliminary simulations as necessary to capture the shape of the shock front thickness. The shockwave front is tracked by thermodynamic properties such as density, pressure and temperature as a function of position along the z direction of the model (Mattsson et al., 2010). Thermodynamic properties are calculated in each bin every 5 ps. For example, the pressure in a bin is calculated by averaging atomic virial stress (Tsai, 1979) over the volume of the bin as,

$$P = \frac{-\Sigma(\sigma_{11} + \sigma_{22} + \sigma_{33})}{3V_{bin}} \tag{3}$$

where σ is the atomic virial stress in units of stress × volume, and V_{bin} is the volume of a small bin. The pressure is computed as the summation of stress over the total number of atoms. Since the atomic stress consists of kinetic and potential energy components, the velocity of the center of mass of each bin is subtracted before the calculation of kinetic energy in that bin to avoid the influence of particle velocity applied in the z direction on the stress calculation. The calculated data is plotted as a function of the bin position, and the discontinuity in thermodynamic properties is identified as the shockwave front. Previous studies by Holian (Holian et al., 1980) and Hess (Hess, 1997) on liquids provided the pressure profile, $P(z_c)$, of a shock front as,

$$P(z_c) = \frac{1}{2}(P_2 + P_1) - \frac{1}{2}(P_2 - P_1)\tanh\left(\frac{2z_c}{L}\right) \tag{4}$$

where P_2 is the pressure in the shocked state, P_1 is the pressure in the unshocked state, L is the thickness of the shock front and $z_c = 0$ corresponds to the center of the shock front. As the shockwave is generated in this work in a sample at thermodynamic equilibrium ($P_1 = 0$) from the momentum mirror at $z = 0$, the pressure profile, $P(z)$, can be re-written as,

$$P(z) = \frac{1}{2}P[1 - \tanh(az + b)] \tag{5}$$

where P is the shock pressure, a describes the shape of the shock front and b refers to the position of the shock front. Using this model, the magnitude and position of the shockwave can be determined.

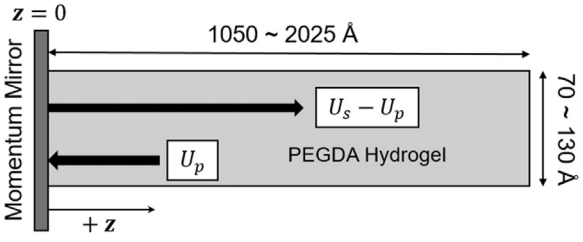

Fig. 2. Schematic of shockwave generations by the momentum mirror method.

3. Shock simulation results

3.1. Shockwave profiles

Fig. 3 shows the shockwave profiles extracted from MD simulations for PEGDA13 hydrogels with 20, 50 and 70 wt% polymer concentrations under 500 and 1000 m/s particle velocities at 0.025 ns. The profiles smoothed by a Savitzky-Golay (SG) filter (Savitzky and Golay, 1964) and the hyperbolic tangent function in Eq. (5) is superimposed onto the simulation data. The shock fronts are clearly identified from the pressure discontinuity. The symmetric tanh function (Eq. (5)) provides a good estimation of the shock front shape at 500 m/s particle velocity. However, some asymmetry is observed at 1000 m/s particle velocity, as the pressure rise is faster at the shock front and more slowly converges behind the shock front than captured by Eq. (5). Such asymmetry increases with polymer concentration at 1000 m/s, where the shock profile of 70 wt% PEGDA exhibits the highest asymmetry (Fig. 3f). This is likely due to increased interaction between PEGDA chains in models with lower water contents.

The shock front thickness is approximated as the difference in z position when $\tanh(az + b)$ reaches ± 0.995 and the shock front center is calculated by $\tanh(az + b) = 0$. The shock velocity is calculated as the mean velocity of the shock front center plus the particle velocity. Data prior to the formation of an equilibrium profile shape is not used in the calculation. All analyses are conducted on three independent models at each particle velocity, and the pressure and shock front thickness presented and analyzed in the sections below are averages over those three models.

In general, the calculated shock front thickness using the symmetric tanh function (shown as the red boxes in Fig. 3) appears to be a reasonable estimation of observed behavior. However, the asymmetry of the shock front at high particle velocities, especially in hydrogels with higher than 50 wt% PEGDA concentration (Fig. 3e and f), does lead to an underestimation of the shock front thickness when using Eq. (5). In the situation of the highest asymmetry, the shock front thickness (approximated via the black box in Fig. 3f) may be 10–30 Å larger than the calculated value using Eq. (5), depending on how it is measured. The implications of this discrepancy will be discussed in Section 3.4.

3.2. Shock Hugoniot relationships

The shock velocity versus particle velocity ($U_s - U_P$) relationships for shock in water and 20–70 wt% PEGDA13 hydrogels are plotted in Fig. 4. The experimental data of 20 wt% ballistic gelatin from Shepherd

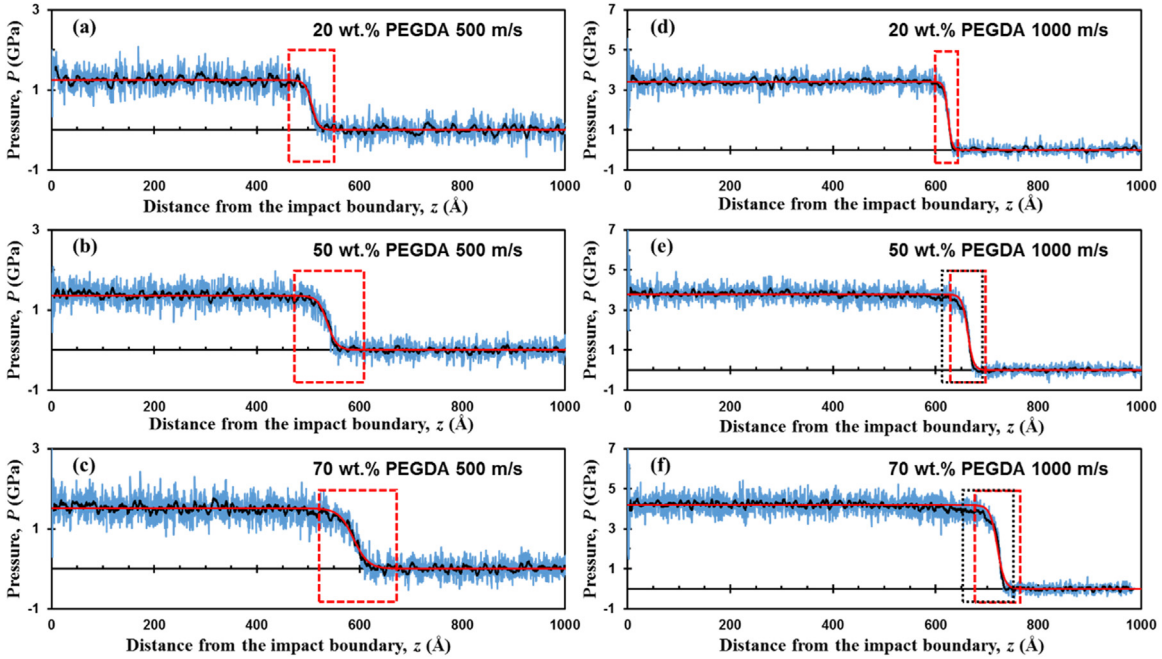

Fig. 3. Shockwave profiles of 20, 50 and 70 wt% PEGDA13 hydrogels under two particle velocities (blue). Black curves are SG filtered profiles. Red lines represent Eq. (5). The calculated shock front thickness are shown by the red box. The black boxes are approximations of the shock front thickness considering the asymmetry in the shockwave shape. (For interpretation of the references to color in this figure legend, the reader is referred to the web version of this article.)

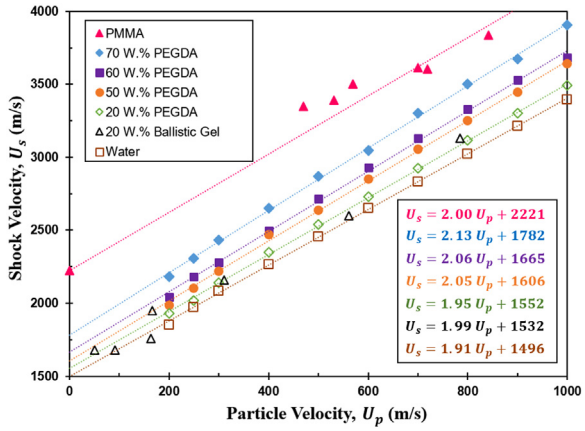

Fig. 4. Comparison between simulation and experiment results on shock velocity versus particle velocity ($U_s - U_p$) Hugoniot for hydrogels with different concentrations.

et al. (2009) and poly(methyl methacrylate) (PMMA) from Marsh (1980) are also included for comparison. The simulation data for hydrogels with 20 wt% PEGDA13 is in good agreement with experimental results from 20 wt% ballistic gelatin (Shepherd et al., 2009), which provides validation of the hydrogel shockwave simulation. The equation of state (EOS) $U_s = SU_p + C_0$ is applied to the $U_s - U_P$ data. The amorphous PMMA polymer with the highest density of 1.186 g/cm^3 has the highest U_s for all values of U_P and water with the lowest density of 0.996 g/cm^3 has the lowest U_s for all values of U_P. As the hydrogel density decreases from 1.131 g/cm^3 to 0.998 g/cm^3, the $U_s - U_P$ relationship indicates a smooth transition from polymer to water behavior, and both the slope S and bulk sound velocity C_0 of hydrogels show decreasing trends (see the table in the lower right corner of Fig. 4). These trends are consistent with the previous observation of Toyoda and Gupta (2014) in 10 wt% and 20 wt% ballistic gelatins. The slope S is commonly referred to as the first pressure derivative of bulk modulus (Grady, 2010), and the bulk sound velocity C_0 is quadratically related to the bulk modulus (Crockett et al., 2004). Thus, the observed changes in S and C_0 indicate that PEGDA hydrogels with higher water concentration exhibit lower bulk modulus. Thus, they are less compressible than PEGDA hydrogels with lower water concentrations. The decrease in compressibility leads to the decrease in S and C_0 and subsequently lower U_s for all values of U_P.

Fig. 5 shows the shock pressure as a function of particle velocity ($P-U_p$) for water and 20–70 wt% PEGDA13 hydrogels along with experimental data for PMMA and 20 wt% ballistic gelatin. The simulation result for the 20 wt% PEGDA13 hydrogel model agrees with the experiment (Shepherd et al., 2009). In the hydrodynamic prediction for shock conditions, a material follows the conservation laws of mass, momentum and energy (Grady, 2017). In Fig. 5, the conservation law of momentum is applied to provide a trend line associated with hydrodynamic prediction,

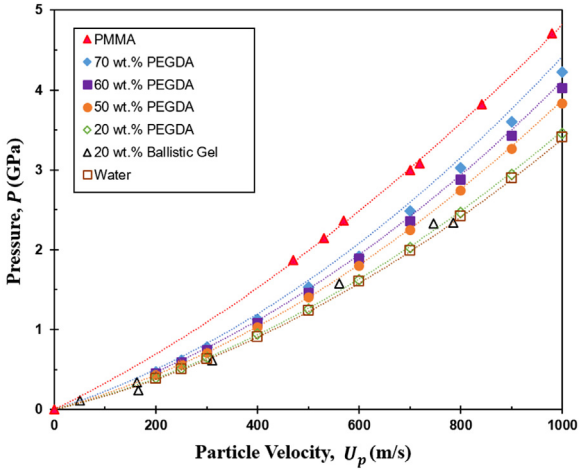

Fig. 5. Shock pressure versus particle velocity ($P-U_p$) Hugoniot for hydrogels with different concentrations. The dotted lines show the hydrodynamic prediction based on hydrogel density and the dots are simulation data points.

$$(P - P_0) = \rho_0 U_s U_p \quad (6)$$

where ρ_0 and P_0 are the initial density and pressure, respectively. Based on the simulation setup, P_0 is treated as 0 GPa. The U_s and U_p are taken from $U_s - U_p$ data (Fig. 4) and the initial density is provided in Table 1. Clearly, the 70 wt% PEGDA13 hydrogel has the largest upward concavity while water has the lowest. This observation is consistent with the results from the $U_s - U_P$ Hugoniot because the slope of the P–U_P curve at each particle velocity is associated with S and C_0. As discussed in the $U_s - U_P$ relationship, the bulk modulus of hydrogels increases with PEGDA concentration, this contributes to the upward shift in P–U_P relationship at higher polymer concentrations. The shock pressure of hydrogels with 60 wt% or lower PEGDA13 concentration follows closely with the hydrodynamic predictions. However, the shock pressure of 70 wt% PEGDA13 hydrogels is 4.5% lower than the hydrodynamic prediction. Note that the 70 wt% PEGDA13 hydrogel model contains 30 wt% water; this is lower than the equilibrium solubility of 34 wt% water reported from experiments (Ju et al., 2009) in PEGDA hydrogels with a DP of 13. Thus, fewer water molecules than the equilibrium state are present in the 70 wt% PEGDA hydrogel likely explaining the deviation between simulation results and hydrodynamic predictions made by Eq. (6).

The pressure versus water concentration ($P - w$) relationship for PEGDA hydrogels with DP of 13 and 23 at particle velocities of 250, 500 and 1000 m/s alongside the experimental data of PMMA (Marsh, 1980) and water (Nagayama et al., 2006) are shown in Fig. 6. No statistically meaningful difference is seen in shock pressure between PEGDA13 and PEGDA23 hydrogels. For all particle velocities, the shock pressure decreases as the water concentration increases. Furthermore, the $P - w$ relationship has increasing nonlinearity with increasing particle velocity. Since no experiment has measured the shock profile in PEGDA polymer, the PMMA polymer is included as an estimation because the two polymers have a similar density. Based on the nonlinearity from Fig. 6, a logarithmic function is proposed for pressure at any U_p as,

$$P = P_{poly} + a_1 \ln(a_2 w + 1) \quad (7)$$

Here, P_{poly} is the shock pressure in pure polymer and w is the water content in the hydrogel. Since the shock pressure in PMMA matches the extrapolation of the nonlinear trend for PEGDA hydrogel to 0 wt% water concentration, it is used for P_{poly} as an estimation. The two boundary conditions of this equation cover the transition of shock pressure from pure water to pure polymer. Data for the PEGDA13 hydrogels are used in the curve-fitting. The curve fit functions are extrapolated to $w = 100$ and compared with experimental results of water (Nagayama et al., 2006). Good agreements are obtained between the extrapolated function and experimental data. Both a_1 and a_2 parameters exhibit decreasing trends with increasing particle velocity, where a_1 decreases from − 0.10 to − 1.08 and a_2 decreases from 0.62 to 0.03 when particle velocities increase from 250 to 1000 m/s.

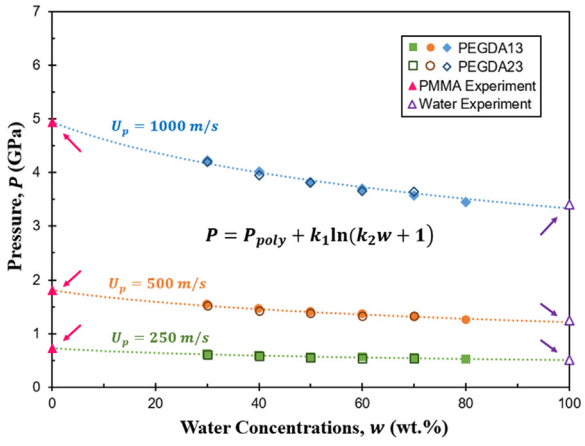

Fig. 6. Shock pressure versus water content for three particle velocities shown. Arrows indicate experimental data for PMMA (Marsh, 1980) and water (Nagayama et al., 2006). The abscissa is in terms of water content in the hydrogel.

3.3. Shock front thickness

While hydrodynamic theory assumes a discontinuity between shocked and unshocked states, a finite width of transition between the two states, defined as the shock front thickness, is observed in experiments (Brown et al., 2007; Hess, 1997) and simulations (Holian, 1998; Holian et al., 1980; Hoover, 1979). Prior research on shockwave structure can be separated based on two material classes: liquid and solid (primarily metal and ceramic materials). Holian (1998) showed that the difference between liquid and solid is the mechanism of atom movements to accommodate the dissipative flow during shockwave propagation. Whereas liquid molecules have no resistance to shear stress and shock propagates by viscous flow, in a solid, the transverse movement is controlled by the intermolecular bonding of the materials. Shockwave structure in hydrogels is expected to be more complex because states of water molecules affect the shock response (Sun and Zhou, 2012), as some water molecules are constrained by the hydrogen bonds from the polymer chains while others remain free to move in the sample. Thus, it is necessary to characterize the influence of water concentrations on the shock front thickness. However, directly applying Eq. (7) to model such relationship is difficult, as there is limited data available on the shock front thickness in a pure polymer L_{poly}. Since the $P - w$ relationship is known, the alternative approach to characterize the shock front thickness is to correlate it with pressure.

In Fig. 7, the shock front thickness versus pressure ($L - P$) relationships of 20–70 wt% PEGDA13 hydrogels under particle velocity from 200 to 1000 m/s are plotted. As polymer concentration and particle velocity are two variables in the figure, their influences are discussed separately. For hydrogels with a constant polymer concentration, the nonlinear decrease in the shock front thickness at higher pressure (solid line) is observed. Such behavior has been recognized in prior shock studies (Holian, 1998; Hess, 1997) and more details will be addressed in the following section. Interestingly, at a fixed particle velocity, as the PEGDA concentration increases, the shock front thickness increases with pressure in a linear fashion (dashed lines). This relationship is seen at all particle velocities from 200 to 1000 m/s, as shown in Fig. 7. To quantitatively characterize the unique correlation, the linear function $L = a_3 P - a_4$ is used to fit simulation results, where the R^2 values of the function in all particle velocities are larger than

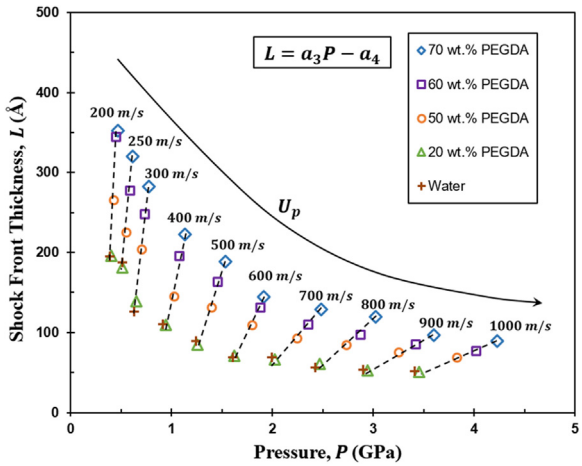

Fig. 7. Shock front thickness-pressure relationship of water and 20–70 wt% PEGDA hydrogels at various particle velocity.

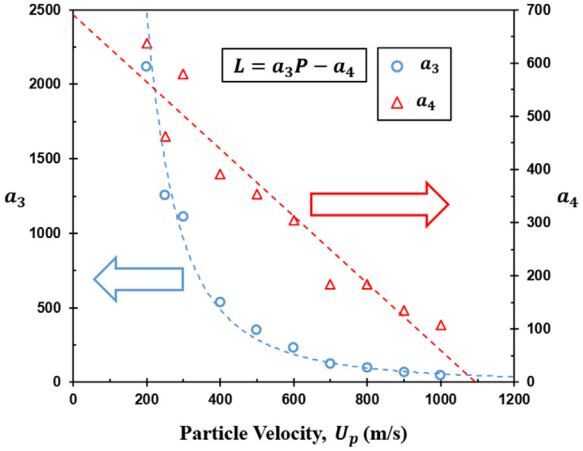

Fig. 8. Trends in linear curve-fit parameters a_3 and a_4 with particle velocity.

0.98. The coefficients a_3 and a_4 are presented in Fig. 8. Clearly, both a_3 and a_4 decrease as particle velocity increases, but with different trends, where a_3 exhibits a nonlinear decaying trend and a_4 changes in a linear fashion. Taking the correlation function L~P, the relationships between shock front thickness and water concentration can be characterized by substituting the linear equations from Figs. 7 and 8 into the pressure versus water content relationships (Eq. (7)) of PEGDA13 hydrogels resulting in,

$$L = a_1 a_3 \log(a_2 w + 1) + (a_3 P_{poly} + a_4) \tag{8}$$

As shown in Fig. 9, the predictions based on Eq. (8) are in decent agreement with simulation data for 1000 and 500 m/s particle velocities. The largest deviation occurs at a particle velocity of 250 m/s, where the magnitude of the oscillations in the pressure due to thermal fluctuations (Fig. 3) begin to influence the precise measurement of the shockwave profile. This could account for the lower accuracy of the model in the shock front thickness versus water concentration relationship at low particle velocity. The PEGDA23 hydrogels in the Fig. 9 exhibit slightly lower average shock front thickness than PEGDA13 hydrogels. As is reported in Table 2, the major difference is that the PEGDA23 hydrogel has a larger average mesh size due to higher degree of polymerization. Such an increase in mesh size enables more water molecules between crosslink junctions and subsequently lower viscosity in hydrogels. This could account for the decrease of shock front thickness in hydrogels with higher DP.

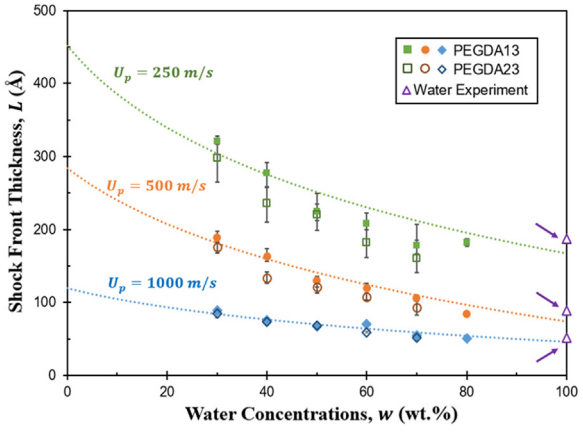

Fig. 9. Shock front thickness versus water content relationship at three particle velocities shown. Arrows indicate reported experimental data for water (Nagayama et al., 2006). The abscissa is in terms of water content in the hydrogel.

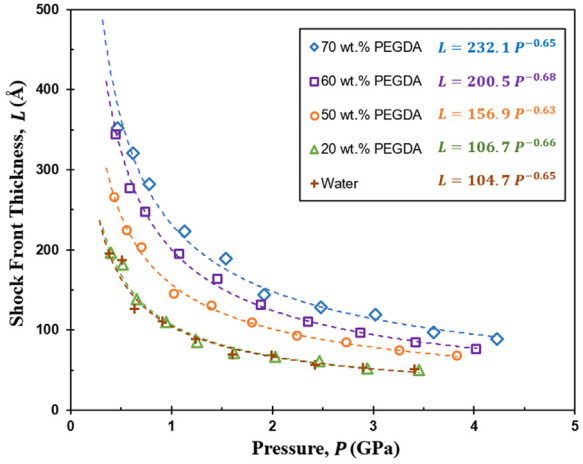

Fig. 10. Shock front thickness-pressure relationship of water and 20–70 wt% PEGDA13 hydrogels. The trend lines are general power-law fit.

3.4. Hydrodynamics and the fourth power-law

As shown in Section 3.3, a nonlinear relationship exists between the shock front thickness and pressure. To study this nonlinearity, the general power-law fit is applied to the data shown in Fig. 8 as,

$$L = C_1 P^{-m_1} \tag{9}$$

Shown in Fig. 10, the general power-law provides a good fit to the $L-P$ simulation data, where the R^2 magnitudes are no less than 0.98. As shown in the legend, the C_1 parameter increases with PEGDA concentrations and the exponent, m_1, which describes the degree of concavity in the $L-P$ relationship, is nearly constant around 0.65. Minimal difference (<2%) is observed in C_1 and m_1 between 20 wt% PEGDA13 hydrogel and water. This suggests that PEGDA13 hydrogels under 20 wt% polymer concentrations have a similar behavior as water during shockwave propagation within this range of particle velocities. However, such similarity disappears at higher polymer concentrations.

In fluid mechanics theory (Landau and Lifshitz, 1987), the extended hydrodynamic function that includes transport properties of the material describes the shock front thickness as,

$$L = 8aV^2\left(\frac{\partial^2 V}{\partial P^2}\right)_s^{-1} P^{-1} \tag{10}$$

where a is positively related to shear viscosity, bulk viscosity and heat conductivity (Hess, 1997), and V is the specific volume. The product of $8aV^2\left(\frac{\partial^2 V}{\partial P^2}\right)_s^{-1}$ is normally considered as a material constant, where Eq. (10) could be written as $L = L_{ref} P_{ref} P^{-1}$ for linear hydrodynamics. The shock responses of water and hydrogels along with the extended hydrodynamic function are plotted in Fig. 11. Clearly, the slopes of the $L-P$ relationships, which are described by the parameter m_1, are consistent for water and hydrogels. This indicates the mechanism of shock deformation is generally independent of water concentration in PEGDA hydrogels. The shock front thickness in water and hydrogels approaches the hydrodynamic approximation at lower shock pressure while the deviation increases at higher magnitudes of shock pressure. A similar deviation was also found in an experimental analysis of shock front thickness in water and liquid methanol by Hess (Hess, 1997), where he proposed a parameter H as the hydrodynamic deviation that converges to 1.0 in the limit of linear hydrodynamics. This deviation is likely caused by changes in viscosity and thermal conductivity of hydrogels at higher pressure and temperature, whereas the extended hydrodynamic theory assumes those transport coefficients are independent of temperature and density (Landau and Lifshitz, 1987). Moreover, MD simulations show that higher PEGDA concentrations lead to higher deviations from a linear hydrodynamics model. This is

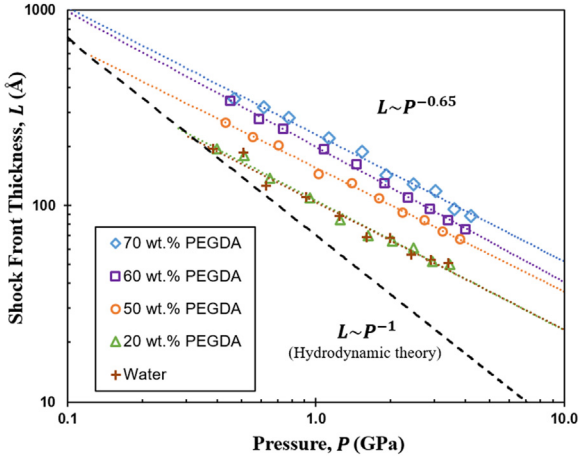

Fig. 11. Shock front thickness-pressure relationship of water and PEGDA13 hydrogels in log-log scale.

associated with the increase of material constant $L_{ref}P_{ref}$ as hydrogels with higher polymer concentrations are expected to have higher viscosity.

To validate these explanations, it is necessary to estimate the transport properties of materials under shock conditions. The numerical solution of such estimation was provided by Grady (1998) as the "artificial viscosity", which accounts for dissipative behaviors during shockwave propagation. The artificial viscosity of a linear $U_s - U_P$ material is calculated as,

$$\eta \cong \frac{1}{4}SP\tau = \frac{1}{4}S\rho_0 U_p L \tag{11}$$

where τ is the rise time of the shockwave. Based on Eq. (11), the artificial viscosity of hydrogels and water are plotted in Fig. 12. Clearly, the artificial viscosity increases with polymer concentration in the hydrogel. This supports data in Fig. 11 that an increase in viscosity leads to larger deviations from linear hydrodynamic theory at higher polymer concentrations. Furthermore, the artificial viscosity increases modestly with particle velocity for water and hydrogels with less than 50 wt% PEGDA. Hydrogels with higher PEGDA concentration show increasing artificial viscosity up to 500 m/s, then a plateau is reached. This validates the previous explanation that an increase in transport properties at higher particle velocities causes the deviation from the extended hydrodynamic theory. The plateau in artificial viscosity at higher particle velocities for hydrogels with greater than 50 wt% PEGDA is due to challenges in computing the shock front thickness, due to presence of asymmetry as explained in Section 3.1. Use of Eq. (5) leads to an underestimated shock front thickness and consequently lower artificial viscosity calculated from Eq. (11) (shown in the top right corner of Fig. 12). Additionally, it is noted that the 20 wt% PEGDA hydrogels share a similar artificial viscosity with water. This provides additional evidence that water and 20 wt% PEGDA hydrogels behave similarly under shock conditions.

The previous discussions of the $L - P$ relationship (Figs. 10–12) show a clear deviation between the MD simulation results and shock front thickness predicted by the theory of fluids (Landau and Lifshitz, 1987). This is somewhat expected as the hydrogels are fluid/solid composites. In solids, the fourth power-law (Grady, 2010) is often observed, which relates the maximum strain rate to the shock pressure, $\dot{\varepsilon}\sim P^4$. The derivation of this relationship by Grady (1981) is based on the assumption of a shock invariant in the form of $A = \partial E \times \partial t$ where the A is the shock invariant, ∂E is the energy difference between shock and isentropic compression and ∂t is the shockwave rise time. It is postulated that A is related to the viscosity of the material because it accounts for the dissipation of energy and the shockwave structure (Gabler et al., 2009). This theory has shown good agreement with shockwave behaviors in metals. However, experimental data shows that the fourth power-law does not accurately describe shock in many composites (Grady, 2010), showing a smaller power-law component.

The $\dot{\varepsilon}-P$ relationship for 20–70 wt% PEGDA hydrogels on a log-log scale is shown in Fig. 13. Here, the volumetric strain rate $\dot{\varepsilon}$ is measured by $\dot{\varepsilon} = U_p/L$ (Holian, 1998). The power-law function $\dot{\varepsilon} = C_2P^{m_2}$ is used as a model for the simulation data. Clearly, the C_2 parameter increases with water concentration while the m_2 parameter is constant around 1.4 regardless of water concentration. Based on experimental results from Brown et al. (2007) and Zhuang et al. (2003), a value between 1 and 2 is also observed in granular and laminated composites.

Clearly, the above results of $L - P$ and $\dot{\varepsilon}-P$ relationships show that hydrogels exhibit a shock response that deviates from both the hydrodynamic prediction of fluids and the fourth power-law relationship in solid materials. The results presented here on PEGDA hydrogels with various water concentrations are the first of its kind and provide a unique insight into the features of shockwave propagation characteristics, specifically focused on the influence of water concentration on shock front thickness, induced pressure and viscosity. Such studies provide guidance when designing surrogates or protecting materials under high velocity impact.

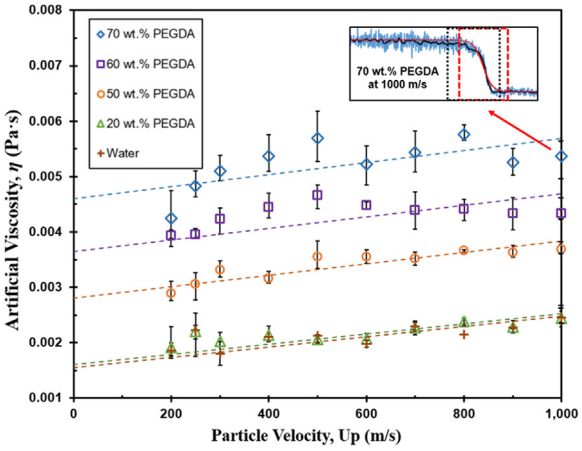

Fig. 12. Plot of artificial viscosity versus particle velocity of water and PEGDA13 hydrogels. The inset shows the underestimation of the shock front thickness using Eq. (5) in the case of 70 wt% PEGDA hydrogel at 1000 m/s.

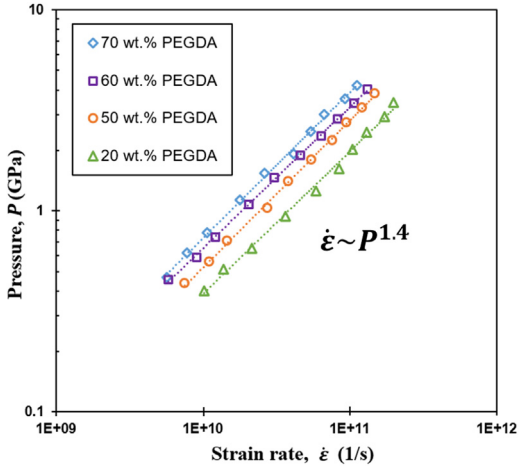

Fig. 13. Plot of pressure versus strain rate in log-log scale for various concentrations of PEGDA13 hydrogels.

4. Conclusions

Nonequilibrium molecular dynamics simulations with the "perfect network" model are performed to investigate the dynamic behavior of PEGDA hydrogels under shockwave propagation. Hydrogel models with PEGDA concentrations from 20 to 70 wt% PEGDA and two different degree of polymerizations are employed to investigate the effect of water concentration on the shock response. The shock Hugoniot of hydrogels are found to be between water and PMMA polymer experimental data, where the magnitude of the shock pressure depends on water concentration, and thus the density. The shock velocity, shock pressure and shock front thickness exhibit a nonlinear increase with polymer concentration in hydrogels, which is attributed to changes in material properties such as bulk modulus, viscosity and heat conductivity. A logarithmic model is proposed to empirically describe the influence of water concentration on shock pressure and shock front thickness. The relationship between shock front thickness and pressure is modeled via a general power-law. Deviations from linear hydrodynamic predictions are observed for hydrogels where the exponent index $m_1 = -0.65$ is found to be independent of water concentration. At lower polymer concentrations (up to 50 wt% PEGDA), the artificial viscosity is found to increase with particle velocity. However, at higher polymer concentrations, a plateau in artificial viscosity is reached when particle velocity exceeds 500 m/s. This plateau is associated with the asymmetry of the shock profile, leading to an underestimation in the calculation of the shock front thickness. The power-law relationship between strain rate and pressure is explored in PEGDA hydrogels. Instead of a value of 4, typical of metals, a value of 1.4 is observed regardless of hydrogel water concentration.

Acknowledgements

This work was supported by the National Science Foundation under Grant No. CMMI-1634188. NY acknowledges support of the University of Florida University Scholars Programs for undergraduate research. The authors acknowledge University of Florida Research Computing for providing computational resources and support that have contributed to the research results reported in this publication.

References

Abascal, J.L.F., Vega, C., 2005. A general purpose model for the condensed phases of water: TIP4P/2005. J. Chem. Phys. 123, 234505. https://doi.org/10.1063/1.2121687.

Anderson, P.A., Betney, M.R., Doyle, H.W., Tully, B., Ventikos, Y., Hawker, N.A., Roy, R.A., 2017. Characterizing shock waves in hydrogel using high speed imaging and a fiber-optic probe hydrophone. Phys. Fluids 29. https://doi.org/10.1063/1.4982062.

Appleby-Thomas, G.J., Hazell, P.J., Sheldon, R.P., Stennett, C., Hameed, A., Wilgeroth, J.M., 2014. The high strain-rate behaviour of selected tissue analogues. J. Mech. Behav. Biomed. Mater. 33, 124–135. https://doi.org/10.1016/j.jmbbm.2013.05.018.

Berendsen, H.J.C., Grigera, J.R., Straatsma, T.P., 1987. The missing term in effective pair potentials. J. Phys. Chem. 91, 6269–6271.

Brown, J.L., Vogler, T.J., Grady, D.E., Reinhart, W.D., Chhabildas, L.C., Thornhill, T.F., 2007. Dynamic compaction of sand. AIP Conf. Proc. 955, 1363–1366. https://doi.org/10.1063/1.2832977.

Crockett, S., Chisolm, E., Wallace, D., 2004. A comparison of theory and experiment of the bulk sound velocity in aluminum using a two-phase EOS. AIP Conf. Proc. 706, 45. https://doi.org/10.1063/1.1780180.

Cronin, D.S., Falzon, C., 2009. Dynamic characterization and simulation of ballistic gelatin. In: Proceedings of the SEM Conference and Exposition on Experimental and Applied Mechanics. ⟨http://sem-proceedings.com/09s/sem.org-SEM-2009-Ann-Conf-s038p04-Dynamic-Characterization-Simulation-Ballistic-Gelatin.pdf%5Cnpapers3://publication/uuid/C4D884DF-7DFF-450E-89E6-50EF916EDEFF⟩.

Demirci, U., Khademhosseini, A., 2016. Gels Handbook: Fundamentals, Properties and Applications. World Scientific Publishing Company, London.

Doman, D.A., Cronin, D.S., Salisbury, C.P., 2006. Characterization of polyurethane rubber at high deformation rates. Exp. Mech. 46, 367–376. https://doi.org/10.1007/s11340-006-6422-8.

Drury, J.L., Mooney, D.J., 2003. Hydrogels for tissue engineering: scaffold design variables and applications. Biomaterials 24, 4337–4351. https://doi.org/10.1016/S0142-9612(03)00340-5.

El-sherbiny, I.M., Yacoub, M.H., 2013. Hydrogel scaffolds for tissue engineering: progress and challenges. Glob. Cardiol. Sci. Pract. 38, 317–342.

Fischer, E.N., Karplus, M., 1996. Simulation of activation free energies in molecular systems. J. Chem. Phys. 105, 1902. https://doi.org/10.1063/1.472061.

Forte, A.E., D'Amico, F., Charalambides, M.N., Dini, D., Williams, J.G., 2015. Modelling and experimental characterisation of the rate dependent fracture properties of gelatine gels. Food Hydrocoll. 46, 180–190. https://doi.org/10.1016/j.foodhyd.2014.12.028.

Gabler, S., Stampfl, J., Koch, T., Seidler, S., Schuller, G., Redl, H., Juras, V., Trattnig, S., Weidisch, R., 2009. Determination of the viscoelastic properties of hydrogels based on polyethylene glycol diacrylate (PEG-DA) and human articular cartilage. Int. J. Mater. Eng. Innov. 1, 3. https://doi.org/10.1504/IJMATEI.2009.024024.

González, M.A., Abascal, J.L.F., 2011. A flexible model for water based on TIP4P/2005. J. Chem. Phys. 135, 224516. https://doi.org/10.1063/1.3663219.

Grady, D., 2017. The nature of structured shock waves. In: Physics of Shock and Impact, Volume 2 Materials and Shock Response. IOP Publishing, Bristol, UK, pp. 1–50.

Grady, D.E., 1981. Strain-rate dependence of the effective viscosity under steady-wave shock compression. Appl. Phys. Lett. 38, 825–826. https://doi.org/10.1063/1.92146.

Grady, D.E., 1998. Shock-wave compression of brittle solids. Mech. Mater. 29, 181–203. https://doi.org/10.1016/S0167-6636(98)00015-5.

Grady, D.E., 2010. Structured shock waves and the fourth-power law. J. Appl. Phys. 107. https://doi.org/10.1063/1.3269720.

Haraguchi, K., 2007. Nanocomposite hydrogels. Curr. Opin. Solid State Mater. Sci. 11, 47–54. https://doi.org/10.1016/j.cossms.2008.05.001.

Hess, S., 1997. On the shock front thickness in water and other molecular liquids. Z. Naturforsch. Sect. A J. Phys. Sci. 52, 213–219.

Hoare, T.R., Kohane, D.S., 2008. Hydrogels in drug delivery: progress and challenges. Polymer 49, 1993–2007. https://doi.org/10.1016/j.polymer.2008.01.027.

Holian, B.L., 1998. Plasticity induced by shock waves in nonequilibrium molecular-dynamics simulations. Science 280, 2085–2088. https://doi.org/10.1126/science.280.5372.2085. (80-.).

Holian, B.L., Hoover, W.G., Moran, B., Straub, G.K., 1980. Shock-wave structure via nonequilibrium molecular dynamics and Navier-Stokes continuum mechanics. Phys. Rev. A 22, 2798–2808. https://doi.org/10.1103/PhysRevA.22.2798.

Hoover, W.G., 1979. Structure of a shock-wave front in a liquid. Phys. Rev. Lett. 42, 1531–1534. https://doi.org/10.1103/PhysRevLett.42.1531.

IAPWS-95. ⟨http://www.iapws.org/relguide/IAPWS-95.html⟩.

Jang, S.S., Goddard, W.A., 2007. Mechanical and transport properties of the poly(ethylene oxide)-poly(acrylic acid) double network hydrogel from molecular dynamic simulations. J. Phys. Chem. B 111, 1729–1737.

Jewett, Andrew. Moltemplate. ⟨http://www.moltemplate.org/⟩.

Jorgensen, W.L., Chandrasekhar, J., Impey, J.D.M.W., Klein, M.L., Jorgensen, W.L., Chandrasekhar, J., Madura, J.D., Impey, R.W., Klein, M.L., 1983. Comparison of simple potential functions for simulating liquid water. J. Chem. Phys. 79, 626. https://doi.org/10.1063/1.445869.

Jorgensen, W.L., Madura, J.D., Swenson, C.J., 1984. Optimized intermolecular potential functions for liquid hydrocarbons. J. Am. Chem. Soc. 106, 6638–6646.

Ju, H., Mccloskey, B.D., Sagle, A.C., Kusuma, V.A., Freeman, B.D., 2009. Preparation and characterization of crosslinked poly(ethylene glycol) diacrylate hydrogels as fouling-resistant membrane coating materials. J. Membr. Sci. J. 330, 180–188. https://doi.org/10.1016/j.memsci.2008.12.054.

Kwon, J., Subhash, G., 2010. Compressive strain rate sensitivity of ballistic gelatin. J. Biomech. 43, 420–425. https://doi.org/10.1016/j.jbiomech.2009.10.008.

LAMMPS. ⟨http://lammps.sandia.gov/⟩.

Landau, L.D., Lifshitz, E.M., 1987. Fluid mechanics. Inst. Phys. Probl. 6, 539. https://doi.org/10.1007/b138775.

Lee, S.G., Brunello, G.F., Jang, S.S., Bucknall, D.G., 2009. Molecular dynamics simulation study of P(VP-co-HEMA) hydrogels: effect of water content on equilibrium structures and mechanical properties. Biomaterials 30, 6130–6141. https://doi.org/10.1016/j.biomaterials.2009.07.035.

Liew, C.C., Inomata, H., Arai, K., 1998. Flexible molecular models for molecular dynamics study of near and supercritical water. Fluid Phase Equilib. 144, 287–298.

Marsh, S.P., 1980. LASL Shock Hugoniot Data, Los Alamos Scientific Series on Dynamic Material Properties, p. 150. ⟨https://dx.doi.org/0-520-04008-2⟩.

Mattsson, T.R., Lane, J.M.D., Cochrane, K.R., Desjarlais, M.P., Thompson, A.P., Pierce, F., Grest, G.S., 2010. First-principles and classical molecular dynamics simulation of shocked polymers. Phys. Rev. B – Condens. Matter Mater. Phys. 81, 1–9. https://doi.org/10.1103/PhysRevB.81.054103.

Muniz, E.C., Geuskens, G., 2001. Compressive elastic modulus of polyacrylamide hydrogels and semi-IPNs with poly(N-isopropylacrylamide). Macromolecules 34, 4480–4484. https://doi.org/10.1021/ma001192l.

Naarayan, S.S., Subhash, G., 2017. Wave propagation in ballistic gelatine. J. Mech. Behav. Biomed. Mater. 68, 32–41. https://doi.org/10.1016/j.jmbbm.2017.01.030.

Nagayama, K., Mori, Y., Motegi, Y., Nakahara, M., 2006. Shock hugoniot compression data for several bio-related materials. AIP Conf. Proc. 845 II, 1547–1550. https://doi.org/10.1063/1.2263621.

Neogi, A., Mitra, N., 2016. Shock induced phase transition of water: molecular dynamics investigation. Phys. Fluids 28, 1. https://doi.org/10.1063/1.4941049.

Okay, O., 2009. General properties of hydrogels. In: Gerlach, G., Arndt, K.-F. (Eds.), Hydrogel Sensors and Actuators: Engineering and Technology, Springer Series on Chemical Sensors and Biosensors. 6 Springer-Verlag, Berlin.

Patel, S.K., Malone, S., Cohen, C., Gillmor, J.R., Colby, R.H., 1992. Elastic modulus and equilibrium swelling of poly(dimethylsiloxane) networks. Macromolecules 25, 5241–5251.

Puoci, F., Curcio, M., 2013. Smart materials for drug delivery. Orient. J. Chem. 29, 861–870. https://doi.org/10.1039/9781849736800.

Richler, D., Rittel, D., 2014. On the testing of the dynamic mechanical properties of soft gelations. Exp. Mech. 54, 805–815. https://doi.org/10.1007/s11340-014-9848-4.

Rizzo, R.C., Jorgensen, W.L., 1999. OPLS All-Atom model for amines: resolution of the amine hydration problem. J. Am. Chem. Soc. 121, 4827–4836.
Savitzky, A., Golay, M.J.E., 1964. Smoothing and differentiation of data by simplified least squares procedures. Anal. Chem. 36, 1627–1639. https://doi.org/10.1021/ac60214a047.
Shepherd, C.J., Appleby-Thomas, G.J., Hazell, P.J., Allsop, D.F., 2009. The dynamic behaviour of ballistic gelatin. AIP Conf. Proc. 1195, 1399–1402. https://doi.org/10.1063/1.3295071.
Sperling, L.H., 2006. Introduction to Physical Polymer Science, 4th Edition. John Wiley & Sons, Hoboken, NJ.
Subhash, G., Liu, Q., Moore, D.F., Ifju, P.G., Haile, M.A., 2011. Concentration dependence of tensile behavior in agarose gel using digital image correlation. Exp. Mech. 51, 255–262. https://doi.org/10.1007/s11340-010-9354-2.
Subhash, G., Kwon, J., Mei, R., Moore, D.F., 2012. Non-Newtonian behavior of ballistic gelatin at high shear rates. Exp. Mech. 52, 551–560. https://doi.org/10.1007/s11340-011-9513-0.
Sun, D., Zhou, J., 2012. Effect of water content on microstructures and oxygen permeation in PSiMA–IPN–PMPC hydrogel: a molecular simulation study. Chem. Eng. Sci. 78, 236–245. https://doi.org/10.1016/j.ces.2011.11.020.
Toyoda, Y., Gupta, Y.M., 2014. Shockless and shock wave compression of ballistic gel to 1.3 GPa. J. Appl. Phys. 116. https://doi.org/10.1063/1.4898679.
Tsai, D.H., 1979. The virial theorem and stress calculation in molecular dynamics. J. Chem. Phys. 70, 1375–1382. https://doi.org/10.1063/1.437577.
Van Duin, A.C.T., Dasgupta, S., Lorant, F., Goddard, W.A., 2001. ReaxFF: a reactive force field for hydrocarbons. J. Phys. Chem. A 105, 9396–9409. https://doi.org/10.1021/jp004368u.
Vliet, T., 1995. Large deformation and fracture behaviour of gels. Faraday Discuss. 101, 359–370.
Witte, R.P., Blake, A.J., Palmer, C., Kao, W.J., 2004. Analysis of poly(ethylene glycol)-diacrylate macromer polymerization within a multicomponent semi-interpenetrating polymer network system. J. Biomed. Mater. Res. Part A 71A, 508–518. https://doi.org/10.1002/jbm.a.30179.
Wu, Y., Joseph, S., Aluru, N.R., 2009. Effect of cross-Linking on the diffusion of water, ions, and small molecules in hydrogels. J. Phys. Chem. B 113, 3512–3520.
Zhuang, S., Ravichandran, G., Grady, D.E., 2003. An experimental investigation of shock wave propagation in periodically layered composites. J. Mech. Phys. Solids 51, 245–265. https://doi.org/10.1016/S0022-5096(02)00100-X.